THE JOURNAL OF BIOLOGICAL CHEMISTRY
Vol. 280, No. 15, Issue of April 15, pp. 15307–15314, 2005

Printed in U.S.A.

The Crystal Structure of the Outer Membrane Protein VceC from the Bacterial Pathogen *Vibrio cholerae* at 1.8 Å Resolution*

Received for publication, January 12, 2005
Published, JBC Papers in Press, January 31, 2005, DOI 10.1074/jbc.M500401200

Luca Federici‡§¶||||, Dijun Du§||, Fabien Walas‡, Hiroyoshi Matsumura‡ ‡‡, Juan Fernandez-Recio‡¶, Kenneth S. McKeegan||, M. Ines Borges-Walmsley||, Ben F. Luisi‡§§, and Adrian R. Walmsley||¶¶**

From the ‡Department of Biochemistry, University of Cambridge, 80 Tennis Court Road, Cambridge CB2 1GA and ||Centre for Infectious Diseases, Wolfson Research Institute, Queen's Campus, University of Durham, Stockton-on-Tees TS17 6BH, United Kingdom

Multidrug resistance in Gram-negative bacteria arises in part from the activities of tripartite drug efflux pumps. In the pathogen *Vibrio cholerae*, one such pump comprises the inner membrane proton antiporter VceB, the periplasmic adaptor VceA, and the outer membrane channel VceC. Here, we report the crystal structure of VceC at 1.8 Å resolution. The trimeric VceC is organized in the crystal lattice within laminar arrays that resemble membranes. A well resolved detergent molecule within this array interacts with the transmembrane β-barrel domain in a fashion that may mimic protein-lipopolysaccharide contacts. Our analyses of the external surfaces of VceC and other channel proteins suggest that different classes of efflux pumps have distinct architectures. We discuss the implications of these findings for mechanisms of drug and protein export.

To expel drugs and other toxic compounds, Gram-negative bacteria use specialized machinery that guides the compounds across two membranes and over the separating interstitial space, known as the periplasm. One type of such transport machinery is the complex formed by an inner membrane proton antiporter, an outer membrane channel, and a periplasmic protein that consolidates the assembly (1, 2). These energy-dependent tripartite pumps extrude actively a variety of noxious compounds from the cytoplasm or inner membrane to the extracellular medium. A number of such pumps have been implicated in multidrug resistance of Gram-negative species, and representative examples that have been well characterized include the *Escherichia coli* AcrAB-TolC and the *Pseudomonas aeruginosa* MexAB-OprM assemblies (3, 4).

Advances are being made in understanding the mechanism of multidrug efflux in Gram-negative bacteria at the level of stereochemistry. To date, high resolution crystal structures have become available for the outer membrane components TolC (5) and OprM (6), the inner membrane proton antiporter AcrB (7, 8), and the periplasmic adaptor MexA (9, 10). Based on these structures, several models have been proposed for the organization of the AcrAB-TolC assembly as a representative efflux pump (9–11). However, the detailed interactions of the components have not been established nor is it clear how the transport of drugs is coupled to proton translocation.

Tripartite pumps are likely to contribute to drug resistance of the Gram-negative pathogen *Vibrio cholerae*, which is the causative agent of the disease cholera. Isolates of *V. cholerae* have been described that are resistant to chemically diverse antibiotics, such as ampicillin, penicillin, streptomycin, nitrofurantoin, and erythromycin, as well as to toxic metals like Pb^{2+} and Zn^{2+} (12). A putative tripartite pump has been identified from *V. cholerae* comprising the inner membrane antiporter VceB, the periplasmic adaptor protein VceA, and the outer membrane channel VceC (13). Although the function of this pump in *V. cholerea* has not been demonstrated, its components were found to collectively complement the multidrug resistance phenotype in *E. coli* null mutants of *TolC*, *EmrA*, and the inner membrane antiporter, *EmrB* (13). Among the compounds to which the VceABC proteins confer resistance in that mutant *E. coli* are the uncoupler cyanide *m*-chlorophenylhydrazone, the detergent sodium deoxycholate, phenylmercuric acetate, and several antibiotics such as chloramphenicol, nalixidic acid, erythromycin, and rifampicin.

The inner membrane component of the *V. cholerae* efflux pump, VceB, belongs to the major facilitator (MF)[1] superfamily of proton antiporters. These transmembrane proteins lack the extensive periplasmic domain that characterizes members of the Root Nodulation and Division (RND) superfamily, which includes the AcrB and MexB inner membrane proteins mentioned above (14). The large periplasmic domains of the RND-based pumps have been proposed to contact directly the other two components of the tripartite pump (11), and it seems likely that the pumps based on the smaller MF proteins must have a very different quaternary organization with distinctive protein-to-protein interactions and different subunit stoichiometry. Notwithstanding these differences between the MF and RND proteins, the outer membrane and membrane fusion protein components of the MF- and RND-based pumps are likely to

* This work was supported in part by the Wellcome Trust. The costs of publication of this article were defrayed in part by the payment of page charges. This article must therefore be hereby marked "*advertisement*" in accordance with 18 U.S.C. Section 1734 solely to indicate this fact.

The atomic coordinates and structure factors (code 1YC9) have been deposited in the Protein Data Bank, Research Collaboratory for Structural Bioinformatics, Rutgers University, New Brunswick, NJ (http://www.rcsb.org/).

§ Both authors contributed equally to this work.
¶ Recipients of Marie Curie Fellowships.
** Recipient of a Wellcome Trust traveling fellowship.
‡‡ Recipient of a Japanese Society for the Promotion of Science postdoctoral fellowship for research abroad (2004).
§§ To whom correspondence may be addressed. E-mail: ben@cryst.bioc.cam.ac.uk.
¶¶ To whom correspondence may be addressed. E-mail: a.r.walmsley@durham.ac.uk.
|||| Present address: Dept. of Biomedical Sciences, University of Chieti, Via Dei Vestini 31, I-66013 Chieti, Italy.

[1] The abbreviations used are: MF, major facilitator; RND, root nodulation and division; β-DDM, β-dodecyl-maltoside; ABC, ATP-binding cassette.

be close structural homologues. For instance, VceA and VceC are predicted to belong to the same families as AcrA and TolC, respectively, even though the sequence conservation is very limited (having ~10% identity).

Here, we report the crystal structure of the outer membrane component VceC at 1.8 Å resolution. Although widely divergent in sequence, VceC has a high degree of structural similarity with *E. coli* TolC and *P. aeruginosa* OprM. All three proteins form channels that are virtually sealed at the periplasmic end in the "resting state," but each is stabilized by completely different sets of side chain interactions. In addition, although the outer membrane porin-like domain is completely sealed in VceC and partially sealed in OprM, it is completely open in TolC. Calculations indicate that the exposed periplasmic surface of VceC is physiochemically distinct from that of TolC, and it is therefore likely that the two proteins form different types of protein-protein interfaces in their respective RND- and MF-type tripartite pumps. This proposal is in accord with the notion that different architectures must underlie the RND- and MF-based pumps. Here, we discuss further the similarities and differences of the TolC, OprM, and VceC channels, and we describe the implications for drug efflux and transmembrane transport of proteins.

EXPERIMENTAL PROCEDURES

Protein Expression and Purification—The *vceC* gene (GenBank™ accession number NP_231052) was amplified by PCR from genomic DNA of the *V. cholerae* vaccine strain CVD101 (forward primer, 5′-CAT ATG AAA AAT AGC GTT CAA ACG GTA GGT TTG-3′, reverse primer, 5′-CTC GAG AGA TTC TGT TGT TTC AAA ACC GCC GCC-3′), which was shown to have an identical sequence to *vceC* from *V. cholerae* strain N16961 (GenBank™ accession number AE004219), and ligated into pGEM-T Easy vector (Promega). After restriction enzyme digestion of the vector with NdeI and XhoI, the resulting *vceC* fragment was then ligated into pET21a (Novagen), generating a construct to express the *vceC* gene with a C-terminal hexahistidine tag. The construct was transformed into *E. coli* strain BL21-AI (Invitrogen).

Cells were grown in an orbital shaker at 37 °C until the culture reached an absorbance, at 600 nm, of 0.5–0.6 and was then induced by the addition of 0.2 mM isopropyl 1-thio-β-D-galactopyranoside and 0.02% L-arabinose at 25 °C, overnight. The cells were harvested by centrifugation, resuspended in buffer A (20 mM Na_2HPO_4, pH 7.4, 300 mM NaCl, 20% glycerol, 5 units/ml DNaseI, 1 tablet/100 ml protease inhibitor mixture tablet), and lysed by three passages through a Constant System Cell Disrupter (15 Kpsi, model Z-plus 1.1 kW; Constant System). Cellular debris were removed by centrifugation at 17,500 × *g* for 30 min at 4 °C, and the supernatant fraction was subjected to ultracentrifugation at 220,000 × *g* for 90 min at 4 °C. The pellet was suspended in buffer B (20 mM Na_2HPO_4, pH 7.4, 300 mM NaCl, 10% glycerol, 0.5 mM Tris(hydroxypropyl) phosphine (THP)) and then freshly prepared β-dodecyl-maltoside (β-DDM) was added to 2%. The mixture was gently stirred at 4 °C for 1.5 h and centrifuged at 220,000 × *g* for 1 h at 4 °C. NaCl was added to the supernatant to a final concentration of 500 mM and imidazole (6 M, pH 7.4) to a concentration of 15 mM. Extracted histidine-tagged VceC was purified by affinity chromatography using a 1-ml HiTrap chelating column (Amersham Biosciences) immobilized with Ni^{2+} equilibrated with buffer C (20 mM Na_2HPO_4, pH 7.4, 500 mM NaCl, 10% glycerol, 0.5 mM THP, 0.2% β-DDM). The column was washed with 100 mM imidazole added to buffer C. Purified VceC was eluted with 500 mM imidazole, 0.2% β-DDM in buffer B.

Buffer exchange of VceC into buffer D (20 mM Tris-HCl, pH 7.8, 100 mM NaCl, 10% glycerol, 0.5 mM THP, 0.2% β-DDM) was carried out on a HiTrap desalting column (Amersham Biosciences). The eluate was loaded onto a 6-ml RESOURCE Q ion exchange column (Amersham Biosciences) equilibrated with buffer D. The column was washed with the same buffer and then eluted with a gradient of 100–400 mM NaCl over 15 column volumes. Fractions containing purified VceC were pooled, diluted 2-fold with buffer D without NaCl, loaded onto the RESOURCE Q column again, and eluted with 300 mM NaCl in the same buffer. N-terminal sequencing of the purified protein revealed that the first amino acid corresponds to residue 43 of the cloned gene.

Site-directed Mutagenesis of VceC—The E92C mutation was introduced into VceC using the QuikChange® site-directed mutagenesis method (Stratagene) with a 37-base PCR primer (sense 5′-CAG CAC TCA CCA TCG TTA TGC ATG GCA ATG GCT CGG C).

Crystallization and Data Collection—The protein was dialyzed against 20 mM HEPES, pH 7.5, 300 mM NaCl, and 0.1% β-DDM. Prior to crystallization, protein was concentrated to 10 mg/ml. Initial crystals were obtained by the hanging drop vapor diffusion method by mixing 1 μl of protein sample on a silinated coverslip with 1 μl of a reservoir solution containing 35% v/v 2,4-methyl-pentanediol, 100 mM HEPES, pH 7.0, and 200 mM NaCl. The coverslip was sealed on a well containing 1.0 ml of the same reservoir solution and equilibrated at 295 K. Crystals appeared after one month and reached a final size of 0.1 × 0.05 × 0.05 mm^3. To facilitate the binding of mercury compounds to the protein for phasing, protein carrying the mutation E92C was produced and purified with the same protocol. The mutant protein proved to crystallize more easily and to yield crystals of bigger size (up to 0.3 × 0.2 × 0.2 mm^3). Several additives and detergents were tested in the crystallization trials to improve the diffraction quality of the crystals. The best results were obtained by the hanging drop method under the following condition: a droplet made of 1 μl of protein solution, 1 μl of reservoir solution, and 1 μl of octyl-β–glucoside 245 mM was equilibrated against a reservoir solution made of 2-methyl-2,4-pentanediol 45% v/v, HEPES 100 mM, pH 7.0, and 200 mM NaCl. Crystals appeared after 2 days and reached their final dimensions after a week. Crystals were directly frozen after looping from the droplet. These crystals belong to the space group P321.

Data were collected at the ID14–4 beamline of the European Synchrotron Radiation Facility (Grenoble). The best data were obtained with a crystal soaked for 24 h with 50 μM phenylmercuribenzoate and frozen. Complete data were collected to the resolution of 1.8 Å. Data were processed and scaled using DENZO and SCALEPACK, respectively (15). Unit cell dimensions together with statistics about the data processing are summarized in Table I.

Structure Solution and Refinement—Two partially occupied mercury sites were found with an anomalous difference Patterson calculated from the derivative data. However, the electron density maps calculated with SIRAS phases from the Hg derivative were not of sufficient quality to allow building of the protein model. The structure was instead solved by Molecular Replacement using a polyalanine model of the *E. coli* TolC protomer (Protein Data Bank accession number 1ek9) (Molrep version 6.2.5 and CNS) (16, 17). The best solutions were obtained using data collected in-house on a VceC-E92C crystal (see Table I). The optimal solution yielded a single protomer in the asymmetric unit in which the trimer was correctly generated by crystallographic symmetry. With this asymmetric unit composition, the solvent content of the crystal is 60%. To refine the model we used the 1.8 Å dataset, collected on the VceC-E92C crystal soaked with mercury. Two procedures were followed in parallel. In one case, the model was built by the automated building procedure implemented in ARP/wARP starting with calculated phases from the molecular replacement solution for a polyalanine model (18). This provided roughly 80% of the model, which was then completed manually. The second procedure involved manual rebuilding of the original polyalanine model using the ARP/wARP map as a guide. Model building was carried out iteratively using COOT (19) and restrained refinement as implemented in REFMAC5 (20). The models from the two procedures converged to virtually the same structure. Density accounting for two partially occupied mercury atoms bound to Cys-92 was found, consistent with the anomalous Fourier calculations. In addition, a molecule of octyl-β–glucoside bridging the β-barrel domains of two symmetry-related molecules could be built. The final model was refined to an *R* factor of 18.9% and an *R*-free of 22.1% and contains residues 63–480 of the cloned coding sequence and 315 water molecules. The first 20 and the last 4 residues of the mature protein were not built due to the absence of clear density. In addition, the loop 288–294 in the equatorial domain could not be modeled due to poor density. The final quality of the model is excellent as judged using PROCHECK (21). Statistics relative to the refinement and the quality of the model are shown in Table I.

Structural superpositions were performed using the program COMPARER (22). The program JOY was used to highlight secondary structure elements in the structural alignment (23). The optimal desolvation areas for VceC and TolC were computed using a variation of the ODA method (24), where the starting points for the generation of optimal surface patches were located at the geometrical center of every surface residue. The program GRASP (25) was used to calculate the electrostatic potential surfaces and to prepare Fig. 4. The figures were otherwise prepared using PYMOL (DeLano Scientific, San Carlos, CA), COOT, and ICM (www.molsoft.com). The coordinates and structure factors were deposited with the Protein Data Bank (accession code 1YC9).

Modeling of the VceC Open State—The sequence of VceC can be split into N- and C-terminal halves that probably arose by gene duplication.

TABLE I

	Native	Hg derivative
	In house	European Synchrotron Radiation Facility at ID14.4
Data collections		
Wavelength (Å)	1.5418	0.9686
Resolution (Å)	26.17–3.30	63.63–1.80
(last shell)	3.42–3.30	1.90–1.80
R_{merge}	0.093(0.367)	0.076(0.419)
Unique reflections	9230	53173
Completeness	99.6 (99.7)	100 (100)
Multiplicity	4.2	8.0
$I/\sigma(I)$	14.6	5.5
Cell dimensions	$a = b = 71.929$ $c = 191.213$	$a = b = 71.458$ $c = 190.702$
Space group	P321	P321
Refinement		
R (working set)		0.1887
R_{free} (test set)		0.2212
Root mean square deviations		
Bond lengths (Å)		0.019
Bond angles (Å)		1.751
Ramachandran statistics		
% of residues in allowed regions		96.2
% of residues in generously allowed		3.8
% of residues in not allowed		0
Model		
Amino acids		410 of 441
Water molecules		315
Octyl-β-glucosides		1
Mercury atoms		2

The N-terminal repeat (residues 63–286) was aligned with the C-terminal repeat (residues 295–480) using CLUSTAL-X (26). The structure of the N-terminal repeat was used as a template for generating a model of the C-terminal repeat, using Modeler version 6.2 (27). We generated 15 models and ranked them by energy and violations from ideal geometry. The best model was further validated using Verify3D (28) and PROCHECK. At this point the model was superimposed to the VceC protomer. As expected the β-barrel domain and the first part of the α-barrel domain were perfectly aligned, whereas the terminal part of helices H7 and H8 adopted an open conformation. A model for the open state of the VceC protomer was obtained by merging the experimental and modeled coordinates.

RESULTS

Overall Fold—The structure of the 442-residue VceC protein from *V. cholerae* was solved by molecular replacement using the *E. coli* TolC structure as a template. The final model accounts for 93% of the mature protein. Missing portions are as follows: (i) the first N-terminal 20 residues, (ii) the last 4 C-terminal residues, and (iii) the loop 288–294 in the "equatorial domain" (which is the outermost group of concentric structural elements that can be seen in Fig. 1*b*). One VceC protomer occupies the asymmetric unit, and the trimer is generated by the crystallographic 3-fold axis. The VceC trimer has a cannon-like shape with a total length of ~140 Å, and the general architecture of the protein is similar to that of TolC (Fig. 1*a*). Two principal domains, a β-domain and an α-domain, are distinguishable in the VceC protomer. The β-barrel domain spans ~40 Å and is the transmembrane portion of the molecule. This β-domain consists of four anti-parallel β-strands organized in a highly twisted and curved β-sheet. Strands 1–2 and 3–4 are connected by two long extracellular loops consisting of 13 and 10 residues, respectively. The sheer number for these self-closing β-sheets (a metric of strand inclination) is the same for TolC, OprM, and VceC.

The α-barrel domain, which protrudes into the periplasm, is composed of six helices. Two of these helices, helices H3 and H7, extend for the entire length of the domain, whereas helices H2-H4 and H6-H8 stack end-to-end and thus resemble pseudo-continuous helices. The six helices forming the α-barrel domain are connected by several segments, which in VceC are mostly unstructured. We distinguish in this region, which has been referred to in TolC as the equatorial domain, the helix H1 and a short helix 3_{10} (G5) that topologically replaces a β-strand and a helix in TolC. In this region the loop 288–294 could not be modeled due to lack of density.

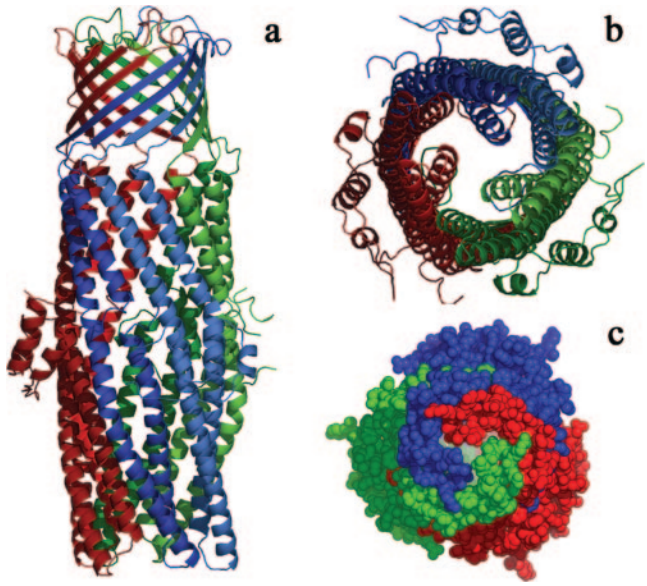

FIG. 1. **Structure of the VceC trimer.** *a*, view perpendicular to the molecular 3-fold axis. The repeat found in the protomer sequence is highlighted by the *dark* and *light blue* coloring of the front protomer. *b*, view of the trimer from the cytoplasmic membrane. *c*, space-filling representation of the trimer from the extracellular space showing the closure of the β-barrel domain.

Interestingly, the VceC trimers pack in laminar arrays in the crystal (Fig. 2*a*). This packing brings the exposed hydrophobic surfaces of the β-barrel together in the same plane and mimics the organization of a planar membrane (commonly referred to as "type I crystal packing"). Within this membrane-like layer, octyl-β–glucoside molecules are found that nestle between two adjacent β-barrel domains. Two such

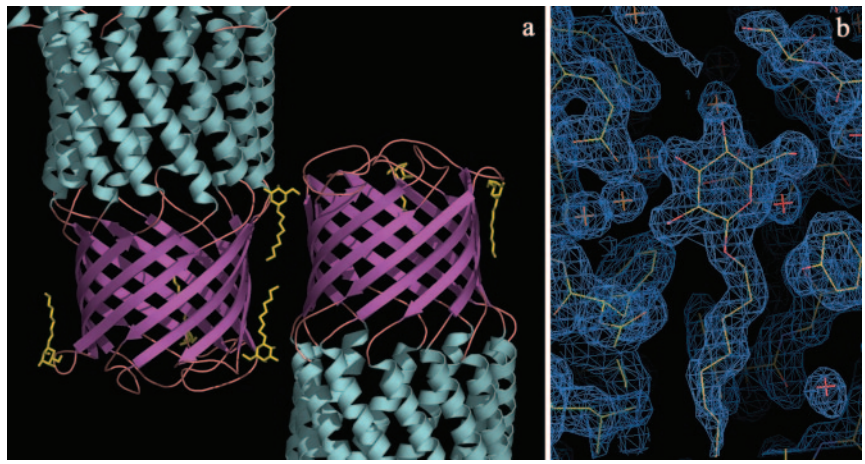

FIG. 2. **The packing of VceC in the crystal lattice.** *a*, laminar packing of VceC in sheets that mimic the lipid bilayer. Two octyl-β-glucoside molecules resemble a bilayer and are related by crystallographic symmetry. *b*, A 2 $F_o - F_c$ electron density map, contoured at 1.5 σ, showing the octyl-β-glucoside molecule at the interface between symmetry-related protomers.

molecules line end-to-end and span the height of the porin-like domain as though they were lipids in the two leaflets of a bilayer membrane (Fig. 2*a*). The detergent molecules make both hydrophobic interactions with the protein through their aliphatic chains and a number of hydrogen bond interactions via their sugar moieties (Fig. 2*b*). Perhaps these contacts mimic protein-lipopolysaccharide interactions that occur in the outer membrane of Gram-negative bacteria.

The α-barrel domain has a length of ~100 Å. The internal diameter is 30 Å and is roughly constant from the equatorial domain to the β-barrel domain. From the equatorial domain to the periplasmic periphery, the channel tapers gradually to an almost complete close. Here, a small pore remains with a diameter of roughly 3.5 Å (Fig. 1*b*). The tapering arises from the superhelical trajectory adopted by the helical pair H7 and H8, which form a coiled-coil that curves toward the symmetry axis.

Like TolC and OprM, the VceC protomer contains a structural repeat. This repeat originated through gene duplication that likely occurred well before the divergence among Gram-negative bacteria. In VceC, the N-terminal half of the protein (residues 63–286) and the C-terminal half (residues 295–480) can be aligned with a sequence identity of 19.8% and superimposed with a root mean square deviation of 2.7 Å between related Cα atoms. In the superimposed structures it is evident that the terminal parts of the coiled-coil helical pair, H3-H4, are less curved than the corresponding segments in the H7-H8 pair, underlying the possibility of two alternative conformations for the protomer. This has implications for the opening mechanism of the channel, as will be discussed later.

Comparison of VceC, TolC, and OprM—The structure of *V. cholerae* VceC was superimposed on the structures of *E. coli* TolC (5) and the *P. aeruginosa* OprM (6), and the structural alignment between the three proteins is shown in Fig. 3*a*. The root mean square deviations between aligned Cα range from 2.0 Å between VceC and TolC to 1.7 Å between VceC and OprM. The root mean square deviation between TolC and OprM was found to be 1.8 Å. These values indicate that VceC is structurally closer to OprM than to TolC. Although the overall fold is well conserved in both the β- and α-barrels (Fig. 3, *b* and *c*), the sequence identity between structurally aligned segments is very low. Only 8.3% of the aligned 386 residues are identical. It is interesting to note that most of these residues are hydrophobic and play structural roles. Among them we find two prolines located at the abrupt turns between the α-barrel helices and the β-barrel strands. A number of conserved alanines and glycines located at the interface between adjacent helices and leucines play a role in the knobs-into-holes intermeshing between coiled-coiled helices.

Electrostatic Properties of the VceC, TolC, and OprM Channels— Fig. 4 shows representations of the electrostatic surface potential of VceC, TolC, and OprM, where one protomer has been removed so that the interior of the channel can be seen. We note that these channel interiors are generally electronegative, but they are strikingly so in the case of VceC, which contains two rings of clustered negative charge. The first ring is located near the equatorial domain and is made by residues Glu-397 and Glu-303, which are conserved in OprM but replaced in TolC by a threonine and a serine, respectively (Fig. 3*a*). Three acidic residues located at the interface between the α- and β-barrels, *i.e.* Asp-153, Asp-115, and Asp-328, form the second and more prominent ring. None of these residues is conserved in TolC, being replaced by a phenylalanine, a glutamine, and a threonine, respectively (Fig. 3*a*). These two rings might attract substrates to the channel exit electrostatically. It is thought that the substrate specificity is mainly provided by the inner membrane component, but the charge distribution of the outer membrane component may facilitate substrate movement across the channel.

A Closed Pore in the β-Barrel Domain—The β-barrel domain has little sequence conservation between VceC, OprM, and TolC; nonetheless, all share the same extent of strand twist, curvature, and inclination. This trajectory requires a periodic pattern with larger residues preferred on the exterior surface and smaller ones on the interior. Although the strands are similar geometrically, the intrastrand loops vary in length and apparent flexibility. When the structure of TolC was determined, it was noted that the β-barrel region was open widely to the extracellular medium (5). Thus, in TolC, the sole constriction for substrates to diffuse into and out of the channel is the closure of the α-barrel. In the VceC structure we find that the loop between β-strands S1 and S2 is 5 residues longer than in TolC and adopts a completely different conformation, resting over the concave face of the barrel (Fig. 3, *a* and *c*). These loops, contributed by the three protomers of the VceC, form a pore that will likely occlude all but the very smallest substrates (Fig. 1*c*). The boundaries of this pore are formed by Ala-134 and Thr-135. The distance between Ala-134 of one protomer and Thr-135 of the closer protomer is 3.8 Å, whereas the distance between Thr-135 from two different protomers is 5.8 Å. These constraints restrict the pore diameter to ~6 Å, whereas the diameter of the corresponding pore in TolC is ~13 Å.

One well characterized substrate of VceC is the chemical uncoupler of oxidative phosphorylation, carbonyl cyanide *m*-chlorophenylhydrazone (CCCP) (13). We manually docked this molecule onto the periplasmic pore constriction of VceC and found that it is too large to freely diffuse through the pore (data

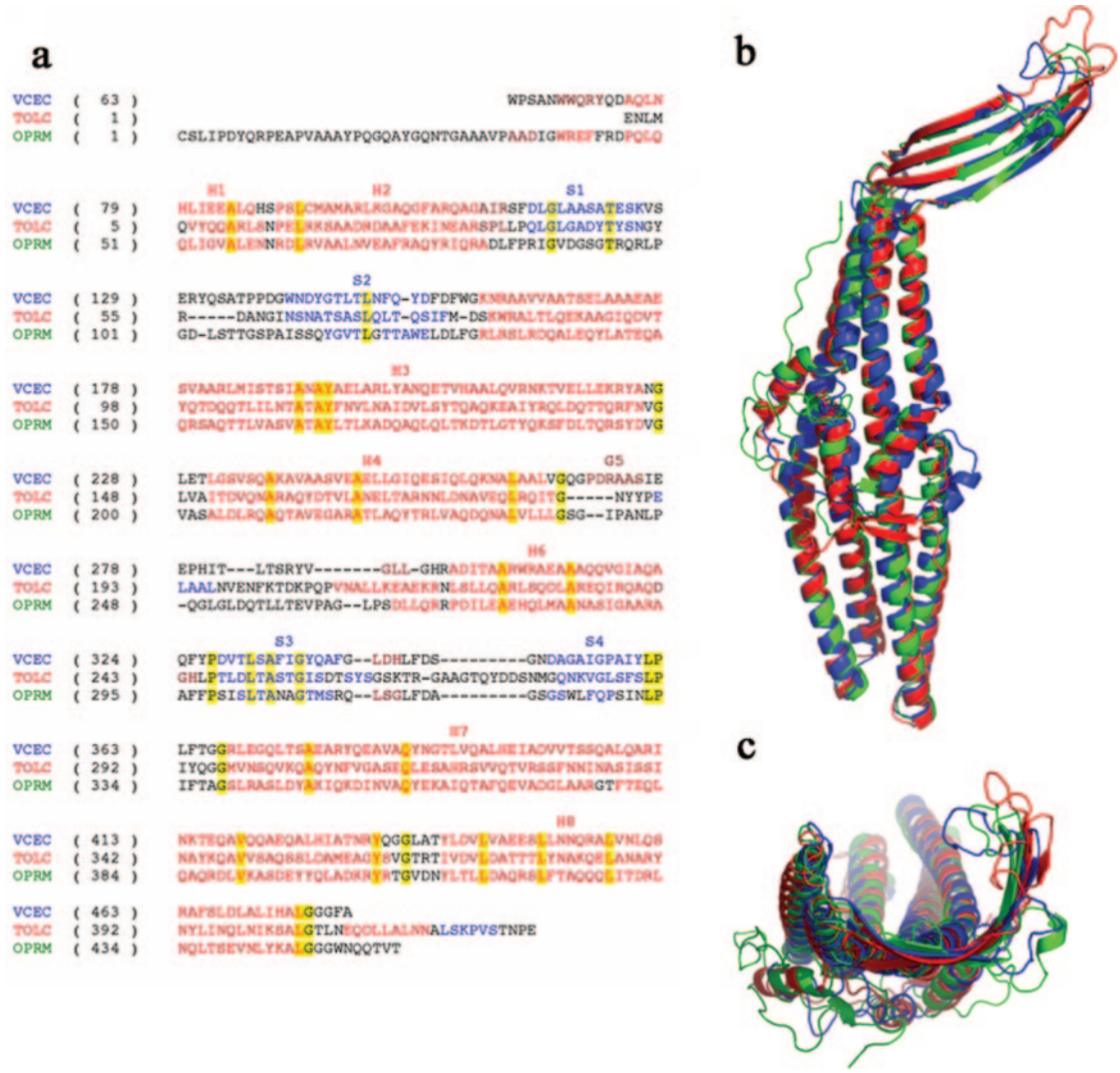

FIG. 3. **Structural comparisons of the outer membrane proteins VceC, TolC, and OprM.** One protomer of the trimer is shown for clarity. *a*, structure-based sequence alignment of the three proteins. The secondary structure elements are annotated and residues colored *red*, *blue*, and *dark red* for helices, strands, and helix 3_{10}, respectively. Identical residues are highlighted in *yellow*. *b*, structural superimposition between VceC (*blue*), TolC (*red*), and OprM (*green*). One protomer of the trimer is shown for clarity. *c*, same as for *panel b* but rotated by 90°. The variation in the intrastrand loops of the β-barrel can be seen.

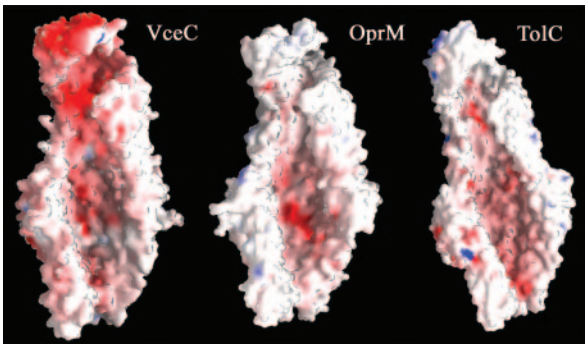

FIG. 4. **Electrostatic charge distribution of VceC, TolC, and OprM.** For clarity, one protomer was removed to show the channel interior. *Red* indicates electronegativity, *blue* electropositivity, and *white* represents neutrality.

not shown). Many of the other known substrates of the VceABC and AcrAB-TolC pumps are even larger than CCCP. It thus seems likely that the transport of these drugs must be linked with opening of the porin domain, but the mechanism is unclear. The opening might be either induced or the consequence of thermal fluctuation.

Closure of the α-Barrel—The VceC channel is almost completely occluded at its periplasmic end. The narrowest point of the channel is 3.4 Å, and a ring formed by Leu-441 of each protomer provides its boundaries. This conformation represents the resting state of the protein. Opening of the channel to allow substrates to enter requires a conformational switch, and this is likely to be driven by interaction with the VceA and VceB partners.

Residues in the loop between helices H7 and H8 mostly constitute the periplasmic pore. Most of these residues are hydrophobic and create a funnel ending with the ring made by Leu-441. Among these residues we find Val-445, Ala-438, and Gly-435. Asp-442 is located near the narrowest point of the funnel and makes a charged ring that might act as an anionic selectivity filter.

In a recent study, Andersen *et al.* (29) identified in TolC a number of interactions that affect the stability of the closed state. In particular, it was shown that two intramonomer hydrogen bonds, between residues Asp-153-Tyr-362 and residues Gln-136-Glu-359, are important. Interestingly, neither of these interactions is conserved in VceC. The TolC Asp-153 corresponds to Ser-233, and the serine side chain interacts with Glu-229 rather than the corresponding tyrosine. This same

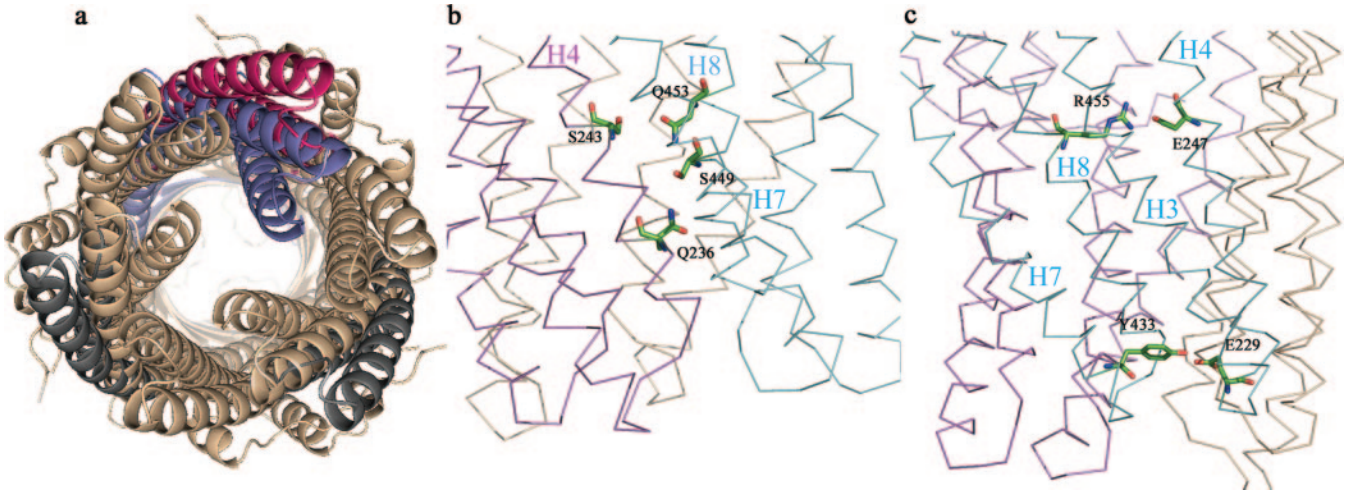

FIG. 5. **Proposed opening mechanism for the VceC channel.** *a*, superimposition of the closed and open states. The moving helices H7 and H8 of one protomer are highlighted in *purple* (closed state) and *magenta* (open state). *b*, polar interactions between protomers that stabilize the closed state. *c*, polar interactions within the same protomer that stabilize the closed state.

Ser-Glu interaction cannot occur in TolC, as Glu-229 is replaced by a valine. The second intramonomer link is also not conserved: the TolC residues Gln-136 and Glu-359 correspond in VceC to Thr-216 and Thr-430, respectively. The side chains of these threonines are too distant to form a hydrogen bond. Moreover, an intermonomer link in TolC is established by a salt bridge interaction between Asp-153 of a monomer and Arg-367 of the adjacent one. Arg-367 also interacts with Thr-152 of the same monomer as Asp-153. None of these intermonomer interactions is possible in VceC where the TolC Asp-153, Arg-367, and Thr-152 are replaced by Ser-233, Ala-438, and Gly-232, respectively.

It thus seems that the VceC channel is stabilized in its closed conformation by a different set of interactions than those found in TolC. To identify such interactions we have modeled the open state of VceC based on the tandem repeat found in the protomer structure of this family of proteins (1, 5). In the proposed open state, the curvature of the helical pair H7-H8 resembles that of H3-H4, and the channel aperture is ~20 Å, thus allowing access to the channel. Fig. 5*a* shows a superposition between the experimental closed state of VceC and the modeled open state. It appears that, upon opening of the channel, the principal structural changes can be attributed to the interfaces between helix H4 of one protomer and helical pair H7-H8 of the adjacent protomer and to the interfaces between helices H3 and H7-H8 of the same protomers. The H4-H7 interface is mostly hydrophobic and 3 residues here, Ile-428, Ala-425, and Val-445, become exposed to the solvent upon opening of the channel. Interestingly 2 of these residues, Ala-425 and Val-445, are replaced in TolC by serine and aspartate. We hypothesize that these residues might play a role in binding the adaptor protein VceA when the pump assembles.

Two intermonomer hydrogen bonds are disrupted in the VceC open state, one between residue pairs Gln-236 and Ser-449 and the second between Ser-243 and Gln-453 (Fig. 5*b*). These interactions are not conserved in TolC, which uses a different set of contacts to stabilize its closed state. Finally two very strong polar interactions were found at the interface between helix H3 and the helical pair H7-H8 of the same protomer, a hydrogen bond between residues Tyr-433 and Glu-229 and a salt bridge between Arg-455 and Glu-247 (Fig. 5*c*). Again, neither of these interactions is conserved in TolC. This analysis demonstrates that within the framework of a very conserved fold, the stabilization of the closed state in TolC and VceC is achieved through different side chain interactions.

DISCUSSION

In this study, we have solved and interpreted the 1.8 Å crystal structure of VceC from *V. cholerae*. This trimeric protein is part of the tripartite pump VceABC that may confer *V. cholerae* with resistance to several antibiotics, detergents, and noxious compounds (13). VceC shares the same overall fold as TolC and OprM, and the three structures can be superimposed with root mean square deviations between corresponding Cα atoms that are below 2.0 Å, despite the very low degree of sequence identity (8.3%). The key elements of the common fold are the regions connecting supersecondary elements (*i.e.* α-helical and β-barrel domains), the periodic pattern of internal and external residues in the porin domain, and the intermeshing residues of the coiled-coil helical interfaces in the periplasmic domain that occur not only within the protomers but also between them in the organization of the trimer.

There is no clear conservation of particular residues that might play defined functional roles. For instance, the residues in TolC that were shown to stabilize the closed state through buried hydrogen bonds and salt bridges (29, 30) are, in fact, not conserved in VceC. Correspondingly, we have identified inter- and intramonomer interactions that might be important in stabilizing the closed state of VceC, and these are not conserved in TolC (see Fig. 5). A number of these interactions are disrupted in VceC when the channel opens, according to our model that predicts a straightening of the coiled-coil helical pair H7-H8. It seems that the different members of this family of outer membrane proteins have evolved different means of affecting the opening and closing of the channel.

The equatorial domain varies in secondary structural composition among the three OM proteins (see Fig. 3*b*). Some of the secondary structure elements found in TolC, such as a β-strand and helix H5 are replaced in VceC by a shorter helix 3_{10} (helix G5), whereas a β-strand and a helix in the C terminus of TolC form an extension that is truncated in OprM and completely absent in VceC (see Fig. 3*a*). No particular functional role has been demonstrated so far for the equatorial domain, although it has been proposed to mediate interactions with the membrane fusion proteins (5). Differences in the equatorial domain between TolC and VceC may reflect structural requirements for binding their adaptor protein partners AcrA and VceA, respectively. We recently noted that, in the modeled open state structure of TolC, a deep groove is formed between the equatorial domains of two adjacent protomers. We hypothesized that the

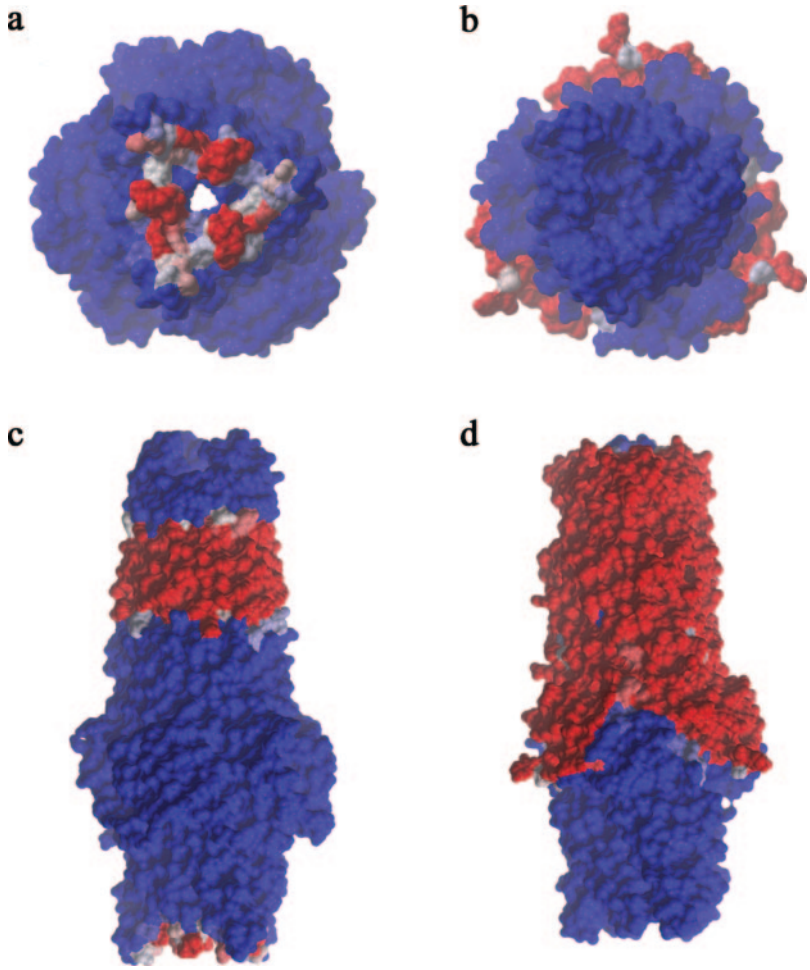

FIG. 6. **Optimal desolvation areas (ODAs) calculated on the surface of TolC and VceC.** Residues are colored according to their corresponding ODA values (*red* for ODA values <15.0 kcal/mol; *white* for ODA values between 15.0 and 10.0 kcal/mol; *blue* otherwise). TolC (*a*) and VceC (*b*) oriented with the 3-fold axis perpendicular to the plane. TolC (*c*) and VceC (*d*) oriented with the 3-fold axis parallel to the plane.

coiled-coil domain of the adaptor periplasmic protein is accommodated in this groove, where it forms a bundle with two helices of TolC. This interaction may trigger the opening of the channel aperture (11, 31). A similar model can be predicted for the open state of VceC, but a different subset of interactions with VceA must be postulated in view of the low degree of conservation between VceC and TolC and, to a lesser extent, between VceA and AcrA.

TolC has been demonstrated to interact *in vivo* with AcrAB (3), and we have recently proposed a model in which TolC and AcrB are in direct contact in a AcrA:AcrB:TolC assembly that has a subunit stoichiometry of 1:1:1. Because the VceB component lacks the extensive periplasmic domain of AcrB, it is expected that the VceA:VceB:VceC pump will differ from the AcrA:AcrB:TolC pump in details of the protein-protein interactions and the subunit stoichiometry. The VceA may form a cylindrical assembly that forms a sheath around the VceC, as proposed for the MexA protein and certain other membrane fusion proteins (1, 9, 11). Thus the VceA:VceB:VceC pump might be expected to have a 3:1:1 subunit stoichiometry. It is not possible, in the absence of a structure for VceB, to propose a complete model for the assembly of the VceA:VceB:VceC pump. However, we have evaluated the surfaces of VceC that are likely to form protein-protein interactions by calculating their optimal desolvation energy. For this calculation, we used the same procedure previously adopted for TolC (11). Whereas the TolC periplasmic end is predicted to intermesh with a protein partner, the corresponding region in VceC appears to lack this potential (see Fig. 6, *a* and *b*). These results suggest that VceB and VceC are not in direct contact in the engaged pump, which is in accord with the expectation that the VceB periplasmic domain is too small to reach the VceC. A striking difference in the optimal desolvation energies is also found in the exterior surfaces of the equatorial domains of the two proteins (see Fig. 6, *c* and *d*). This area is predicted to be a protein interaction site in VceC, but not in TolC, and it is likely to be the site of interaction with the adaptor protein VceA.

Our structural comparisons of VceC, TolC, and OprM suggest that the functional important residues vary between the different members of the TolC family. This divergence reflects not only the different architectures of the three main classes of efflux pumps but also the tremendous co-variation of the components within a class. The TolC family members are involved in different classes of efflux or protein export pumps based on the MF, RND, and ABC inner membrane proteins. It seems very likely that the architectures and subunit stoichiometry will differ between the three classes of pumps, and thus variation of surface residues will have occurred to permit specific matches to the cognate partners. Within a pump class, where the tripartite architecture is expected to be maintained, patterns of co-variation conserve the protein-to-protein interactions even though they differ in detail.

Substrate specificity in tripartite pumps is likely to be provided by the inner membrane component (8). Once delivered into the outer membrane channel, substrates should be able to freely diffuse through the channel. By analyzing the electrostatic potential surfaces of VceC, OprM, and TolC, we noted that the interior of these three channels is generally electronegative. In the case of VceC, we find two negative rings located approximately in the middle of the channel and at the boundaries between the α- and β-barrel domains, respectively. This second ring in particular, which is not seen in TolC and

OprM, is conveniently located to attract positively charged drugs into the outer membrane pore, facilitating their movement along the channel (see Fig. 4). The question remains as to how negatively charged substrates of the VceABC pump, such as nalixidic acid, might diffuse into the repulsive channel. Perhaps they are bound to counter-ions when crossing the channel or are expelled with a pulse of protons.

One striking characteristic of VceC is the presence of a pore at the end of the β-barrel domain (see Figs. 1*c* and 3*c*). The pore is formed by the loops between strands S1 and S2 of each protomer. These loops are longer than in TolC and OprM and are oriented so as to rest upon the porin-like domain, providing only a small passage with a diameter of ~6.0 Å. This diameter is too small to allow the diffusion of antibiotic compounds into and out of the channel. This constriction is likely to affect passage of diffusing substrates. In the OprM structure, the loop region has well defined density only in one of the two molecules in the asymmetric unit, suggesting conformational flexibility in this area that may account for the ability of substrates to easily diffuse out of the pore (6). The loop region is, however, very well defined in the VceC structure, with thermal factors in the same range of the contiguous β-strands. These loops may play a role in controlling the diffusion of substrates, either as a kinetic barrier that opens with thermal fluctuation or as a gate that might be opened upon induction. For instance, Thr-135 at the boundaries of the pore might interact with selected substrates, and this could in turn promote pore opening. Such an inducible pore might provide certain advantages. For instance, it is known that the TolC protein is the conduit for the bactericidal colicin E1 to gain access into the host cell (32), so perhaps the outer membrane pore serves as a barrier against the entry of similar toxins.

Finally, in this work we report the first, to our knowledge, crystallographic visualization of a detergent bilayer whereby two molecules of octyl-β-glucoside, related by crystallographic symmetry, line end-to-end. These molecules establish both polar interactions with their sugar moieties and apolar interactions with their aliphatic chains, bridging two VceC protomers, in the same way that is expected for lipopolysaccharides of the bacterial outer membrane.

Acknowledgments—We thank Len Packman and Mike Weldman (Protein Nucleic Acid Chemistry Facility, Department of Biochemistry, University of Cambridge) for protein analyses. We thank the staff of the European Synchrotron Radiation Facility for kind assistance and use of facilities.

REFERENCES

1. Sharff, A., Fanutti, C., Shi, J., Calladine, C., and Luisi, B. (2001) *Eur. J. Biochem.* **268,** 5011–5026
2. Borges-Walmsley, M. I., McKeegan, K. S., and Walmsley, A. R. (2003) *Biochem. J.* **376,** 313–338
3. Tikhonova, E. B., and Zgurskaya, H. I. (2004) *J. Biol. Chem.* **279,** 32116–32124
4. Li, X. Z., and Poole, K. (2001) *J. Bacteriol.* **183,** 12–27
5. Koronakis, V., Sharff, A., Koronakis, E., Luisi, B., and Hughes, C. (2000) *Nature* **405,** 914–919
6. Akama, H., Kanemaki, M., Yoshimura, M., Tsukihara, T., Kashiwagi, T., Yoneyama, H., Narita, S. I., Nakagawa, A., and Nakae, T. (2004) *J. Biol. Chem.* **279,** 52816–52819
7. Murakami, S., Nakashima, R., Yamashita, E., and Yamaguchi, A. (2002) *Nature* **419,** 587–593
8. Yu, E. W., McDermott, G., Zgurskaya, H. I., Nikaido, H., and Koshland, D. E., Jr. (2003) *Science* **300,** 976–980
9. Higgins, M. K., Bokma, E., Koronakis, E., Hughes, C., and, and Koronakis, V. (2004) *Proc. Natl. Acad. Sci. U. S. A.* **101,** 9994–9999
10. Akama, H., Matsuura, T., Kashiwagi, S., Yoneyama, H., Narita, S., Tsukihara, T., Nakagawa, A., and Nakae, T. (2004) *J. Biol. Chem.* **279,** 25939–25942
11. Fernandez-Recio, J., Walas, F., Federici, L., Venkatesh Pratap, J., Bavro, V. N., Miguel, R., Mizuguchi, K., and Luisi, B. (2004) *FEBS Lett.* **578,** 5–9
12. Choudhury, P., and Kumar, R. (1996) *Indian J. Med. Res.* **104,** 148–151
13. Colmer, J. A., Fralick, J. A., and Hamood, A. N. (1998) *Mol. Microbiol.* **27,** 63–72
14. Paulsen, I. T., Brown, M. H., and Skurray, R. A. (1996) *Microbiol. Rev.* **60,** 575–608
15. Otwinowski, Z., and Minor, W. (1997) *Methods Enzymol.* **276,** 307–326
16. Vagin, A., and Teplyakov, A. (2000) *Acta Crystallogr. Sect. D Biol. Crystallogr.* **56,** 1622–1624
17. Brunger, A. T., Adams, P. D., Clore, G. M., DeLano, W. L., Gros, P., Grosse-Kunstleve, R. W., Jiang, J. S., Kuszewski, J., Nilges, M., Pannu, N. S., Read, R. J., Rice, L. M., Simonson, T., and Warren, G. L. (1998) *Acta Crystallogr. Sect. D Biol. Crystallogr.* **54,** 905–921
18. Perrakis, A., Harkiolaki, M., Wilson, K. S., and Lamzin, V. S. (2001) *Acta Crystallogr. Sect. D Biol. Crystallogr.* **57,** 1445–1450
19. Emsley, P., and Cowtan, K. (2004) *Acta Crystallogr. Sect. D Biol. Crystallogr.* **60,** 2126–2132
20. Murshudov, G. N., Vagin, A. A., Lebedev, A., Wilson, K. S., and Dodson, E. J. (1999) *Acta Crystallogr. Sect. D Biol. Crystallogr.* **55,** 247–255
21. Laskowski, R. A., Moss, D. S., and Thornton J. M. (1993) *J. Mol. Biol.* **231,** 1049–1067
22. Zhu, Z. Y., Sali, A., and Blundell, T. L. (1992) *Protein Eng.* **5,** 43–51
23. Mizuguchi, K., Deane, C. M., Blundell, T. L., Johnson, M. S., and Overington, J. P. (1998) *Bioinformatics* **14,** 617–623
24. Fernandez-Recio, J., Totrov, M., Skorodumov, C., and Abagyan, R. (2004) *Proteins* **58,** 134–143
25. Nicholls, A., Sharp, K. A., and Honig, B. (1991) *Proteins* **11,** 281–296
26. Thompson, J. D., Gibson, T. J., Plewniak, F., Jeanmougin, F., and Higgins, D. G. (1997) *Nucleic Acids Res.* **25,** 4876–4882
27. Fiser, A., and Sali, A. (2003) *Methods Enzymol.* **374,** 461–491
28. Eisenberg, D., Luthy, R., and Bowie, J. U. (1997) *Methods Enzymol.* **277,** 396–404
29. Andersen, C., Koronakis, E., Bokma, E., Eswaran, J., Humphreys, D., Hughes, C., and Koronakis, V. (2002) *Proc. Natl. Acad. Sci. U. S. A.* **99,** 11103–11108
30. Andersen, C., Koronakis, E., Hughes, C., and Koronakis, V. (2002) *Mol. Microbiol.* **44,** 1131–1139
31. Federici, L., Walas, F., and Luisi, B. (2004) *Curr. Sci. INDIA* **87,** 190–197
32. Zakharov, S. D., and Cramer, W. A. (2002) *Biochim. Biophys. Acta* **1165,** 333–346

The Crystal Structure of the Outer Membrane Protein VceC from the Bacterial Pathogen *Vibrio cholerae* at 1.8 Å Resolution

Luca Federici, Dijun Du, Fabien Walas, Hiroyoshi Matsumura, Juan Fernandez-Recio, Kenneth S. McKeegan, M. Ines Borges-Walmsley, Ben F. Luisi and Adrian R. Walmsley

J. Biol. Chem. 2005, 280:15307-15314.
doi: 10.1074/jbc.M500401200 originally published online January 31, 2005
